Simulation results of a 70-degree SPIF formed cone

Carlos Felipe Guzmán*
Department ArGEnCo, Université de Liège, Belgium

June 3, 2013

Contents

*cf.guzman@ulg.ac.be

1 Description

1.1 Geometry and material

The Fig. 1 shows a 70° wall angle cone formed by SPIF. The sheet material is an Aluminum AA3003-O of 1.2 mm thickness. The angle is chosen because is near the failure angle, which is 71° for this particular geometry and material [Duflou et al., 2008]. The tool is a 10 mm sphere, and the tool path is composed of 60 contours with a 0.5 mm stepdown, obtaining a 30mm final depth.

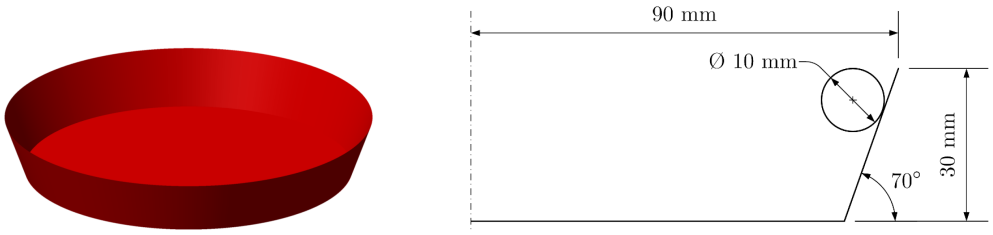

Figure 1: Target geometry.

1.2 Finite element model

The 8-node SSH3D element is used, with 4 integration point in the plane and 5 through the thickness. The element uses 24 EAS modes and the second version of ANS. Two meshes are used: a coarse mesh with 4484 nodes and 3064 elements and a fine mesh with 4492 elements.

As the cone is clamped, the nodes of the outer circumferential part are completely fixed. In the other edges, rotational boundary conditions are assumed.

1.3 Constitutive law

A J_2 isotropic plasticity model plus mixed isotropic/kinematic hardening is used during the simulations. Two set of parameters are used, being the isotropic hardening and the identification procedure the difference between them.

The first set uses a Swift hardening with parameters identified using classical tests (tensile test and monotonic and Bauschinger shear test), while the second set uses a Voce law and parameters using also the classical tests,

but plus an indent test [Henrard et al., 2010]. The Table 1 shows the used parameters.

Table 1: Set of parameters used during the simulations [Henrard et al., 2010].

	Set2 Swift/Ziegler	Set8 Voce/Ziegler
K	146.7	89
n	0.229	22.5
ϵ_0/σ_0	1.5e-3	20
C_A	240.6	11.2
G_A	83	0

2 Results

Despite the long CPU time, the simulation with Set2 did not present any convergence problems. Nevertheless, the Set8 was surprisingly slower and a lot of convergence problems arised. So only the results for the coarse mesh of Set8 are shown, even if they are not complete.

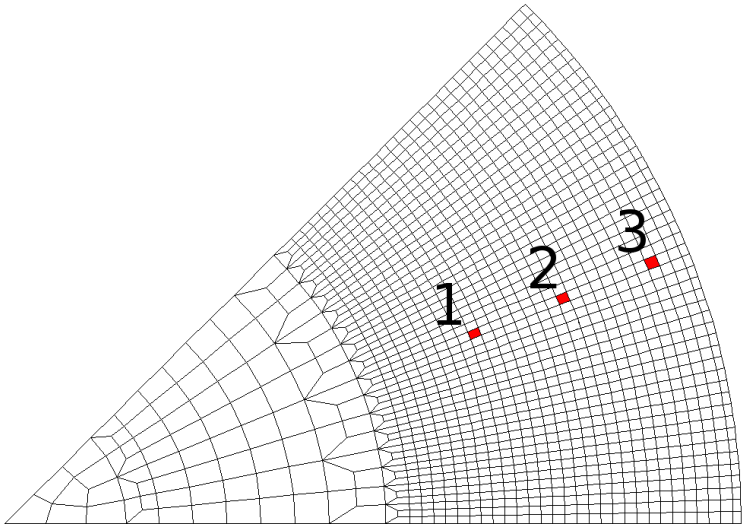

Figure 2: Finite element mesh depicting the three selected elements.

2.1 Shape

There is no influence of the material parameters on the shape prediction. The results are obtained from the nodal displacement at a transversal cut (Fig. 3), and they are shown in Fig. 4.

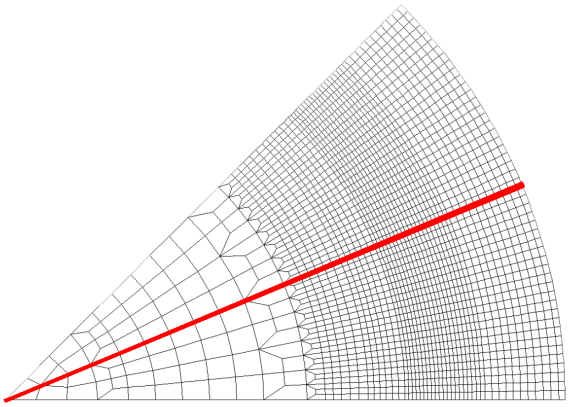

Figure 3: Transversal cut used to obtained the nodal displacements.

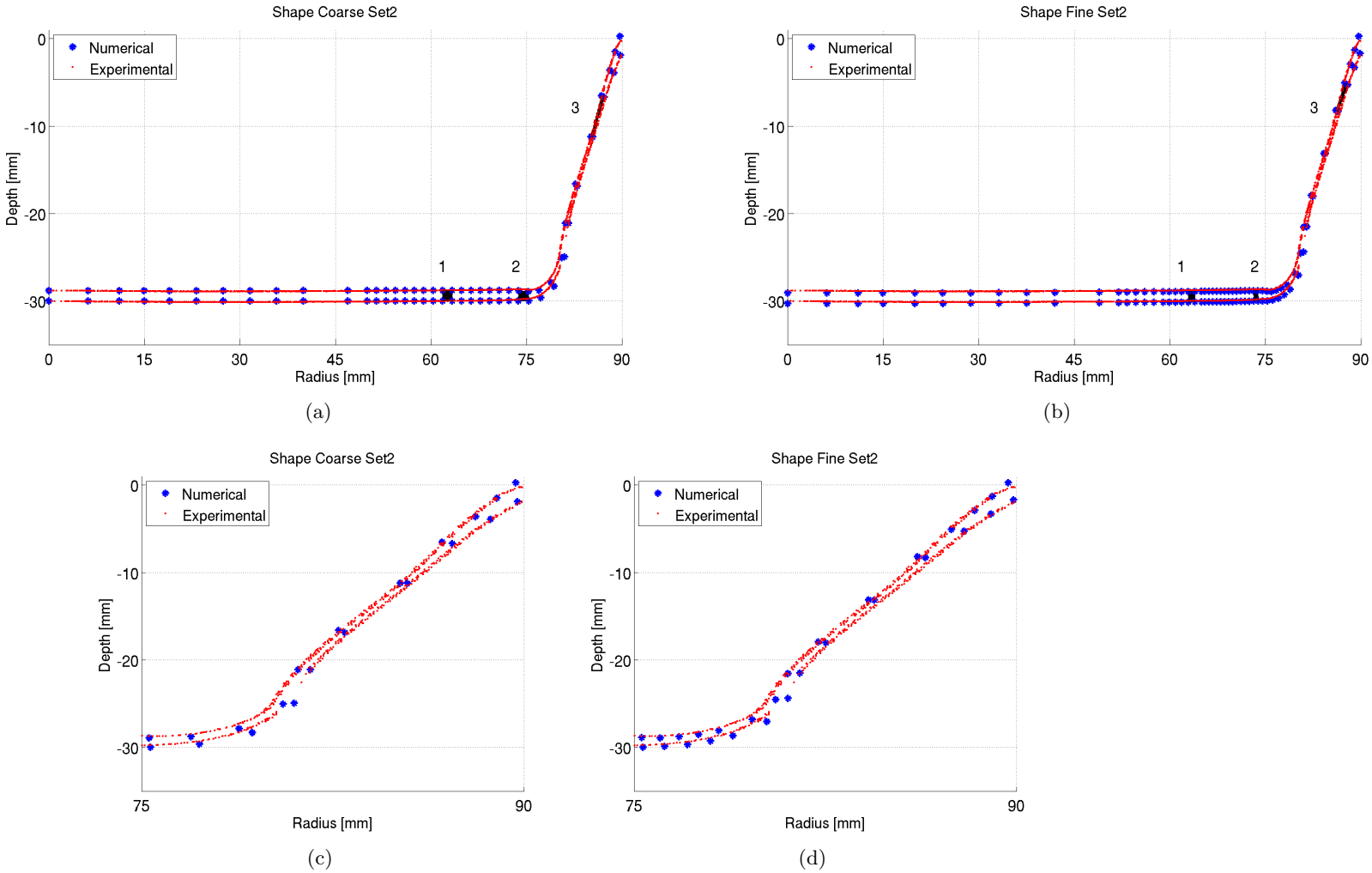

Figure 4: FEA results (blue) and experimental (red). The Fig. 4(c) and Fig. 4(d) shows a zoom into the wall zone, depicted in a different scale for better analysis.

The shape match very well in both the upper and bottom layer with the experimental measurements.

2.2 Thickness

The thickness is calculated following a simple procedure, shown in Fig. 5. This consists in a normal vector from the upper layer towards the bottom layer, and taking the magnitude as the thickness. The results are shown in Fig. 6.

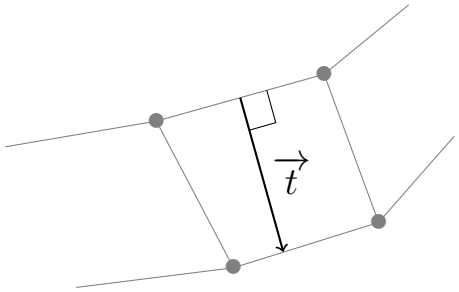

Figure 5: Thickness calculation method used for solid elements.

The results match quite well for both meshes. Neverthless, and because of the mesh refinement in the deformed zone, the fine mesh is more accurate when predicting the minimal thickness. The predicted minimal thickness is 0.27 mm, while the experimental is 0.28 mm.

2.3 Forces

The force evolution is obtained as the reactions forces acting on the tool during the process. To avoid the noise due to *edge effects* and the modified tool motion adapted to the symmetry conditions, an average value of the force at the central third part of the pie is used and depicted in Fig. 9. The evolution is shown in Fig. 8.

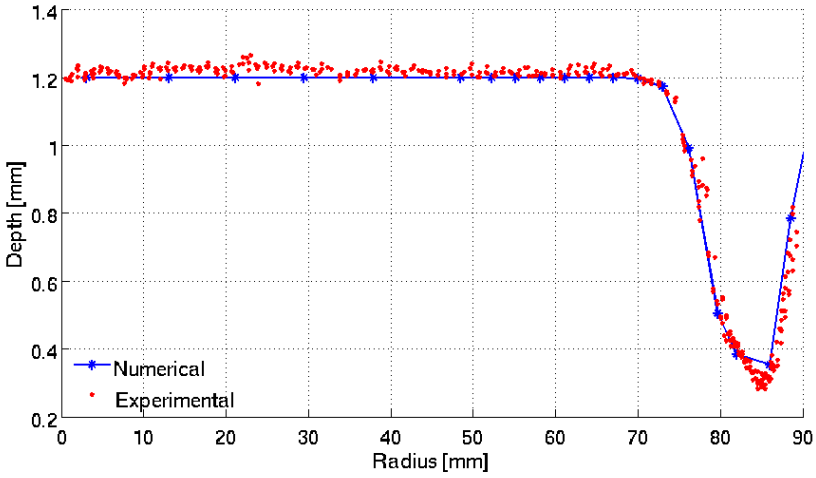

(a) Coarse mesh.

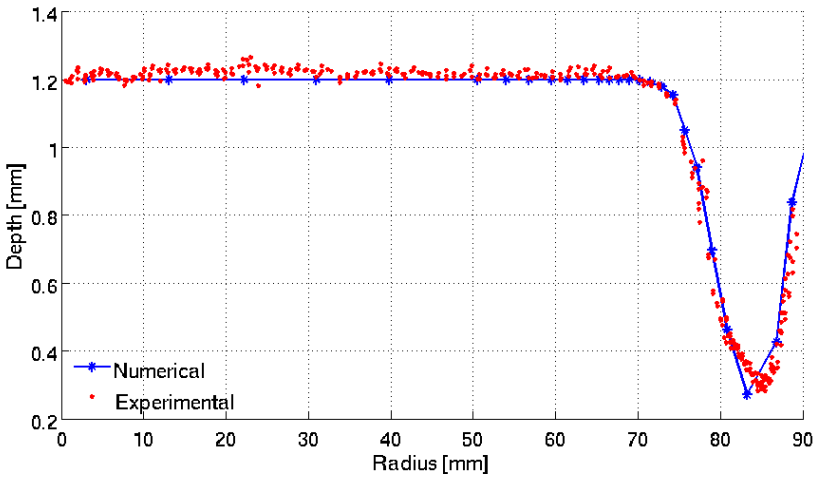

(b) Fine mesh.

Figure 6: Comparison of the thickness distribution in a transveral cut between experimental measurements and numerical predictions, for two different meshes.

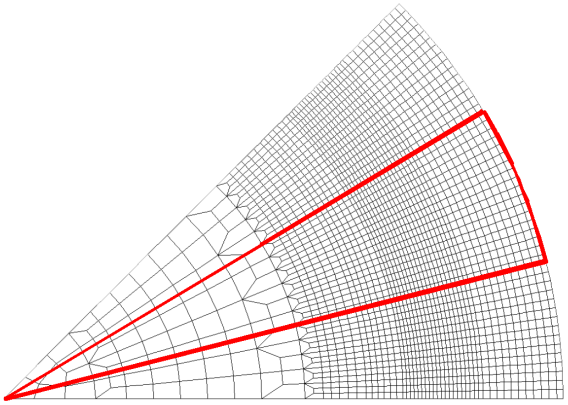

Figure 7: Zone used to obtain the average values of the force.

The analytical formula proposed by Aerens gives values F_s =382.3 N (steady state) and F_p = 596.9 N. The finite element simulations are far lower as was previously observed for this same element for the line test and the two-slope pyramid. Any further work about SPIF and the SSH3D should address this issue.

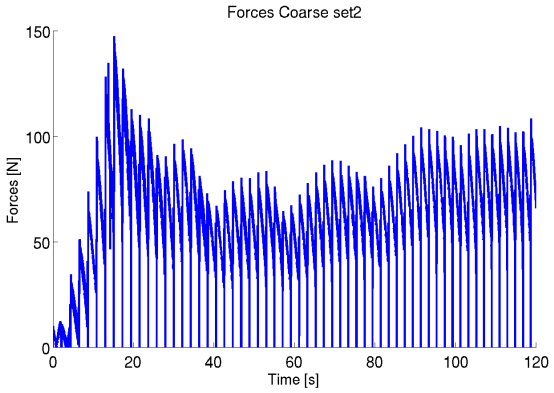

(a) Coarse mesh, set2.

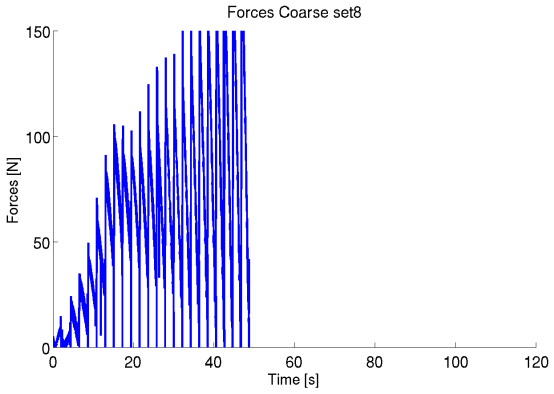

(b) Coarse mesh, set8.

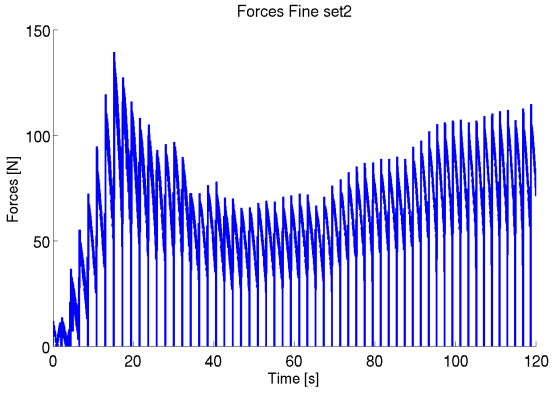

(c) Fine mesh, set2.

Figure 8: Tool reaction during the process.

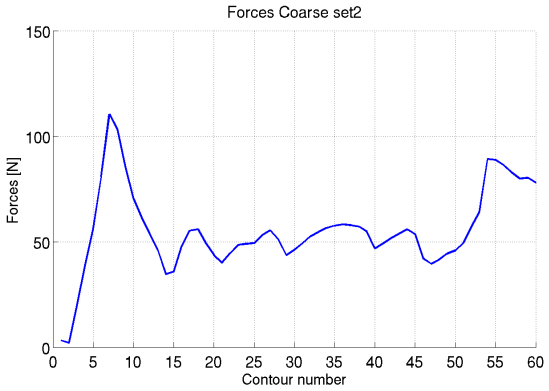

(a) Coarse mesh, set2.

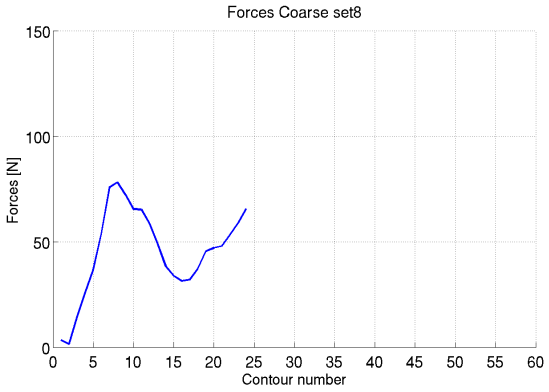

(b) Coarse mesh, set8.

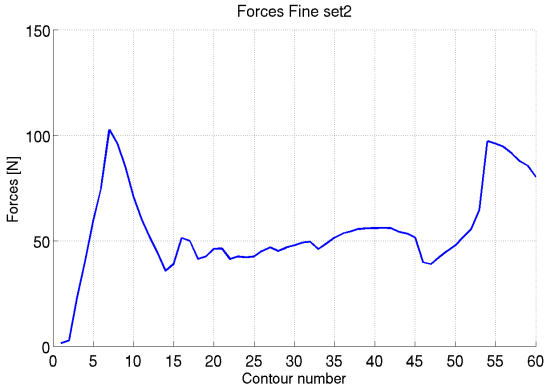

(c) Fine mesh, set2.

Figure 9: Average tool reaction during the process.

3 State variables

The evolution of the triaxiality (Eq. 1) and the normalized third invariant (Eq. 2) are analyzed for the three elements depicted in Fig. 2. Three integration points (being IP1 closer to the bottom surface) are plotted.

$$T = \frac{\sigma_h}{\sigma_{eq}} \tag{1}$$

$$X = \cos 3\xi_{Lode} = \pm\frac{27}{2}\frac{J_3}{\sigma_{eq}^3} \qquad -1 \leq X \leq 1 \tag{2}$$

From this last equation, by assuming $T = 0$ $X = \pm 1$ is somewhat similar to an axisymmetric stress state while $X = 0$ is closer to in-plane shear. In plane stress conditions, there is a direct relation between triaxiality and the third invariant:

$$X(T) = \cos 3\theta = -\frac{27}{2}T\left(T^2 - \frac{1}{3}\right) \tag{3}$$

Because of the *noise* introduced by the edge effects of the symmetry assumptions, the results are between the edges depicted in Fig. 7. To know in what stage of the deformation the elements are, the equivalent plastic strain is plotted in Fig. 10. A new element is added (element 4) that will be explained later, while in element 1 the plastic strain is negligible. Only results from set2 are shown hereafter.

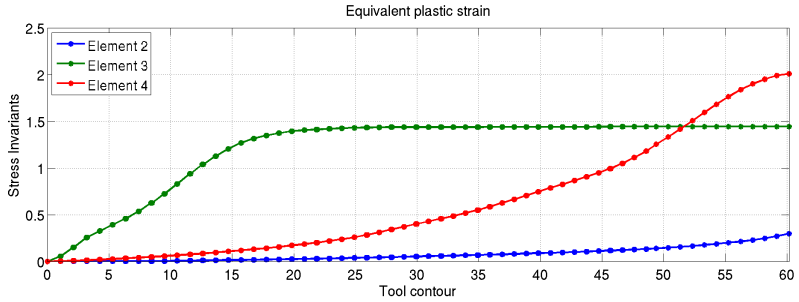

Figure 10: Equivalent plastic strain for three selected elements.

3.1 Coarse mesh, Set2

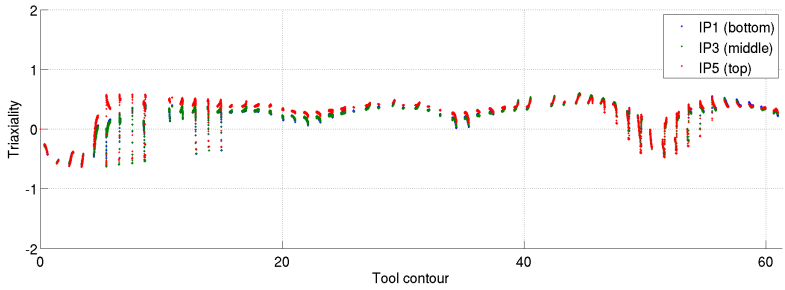

(a) Element 1.

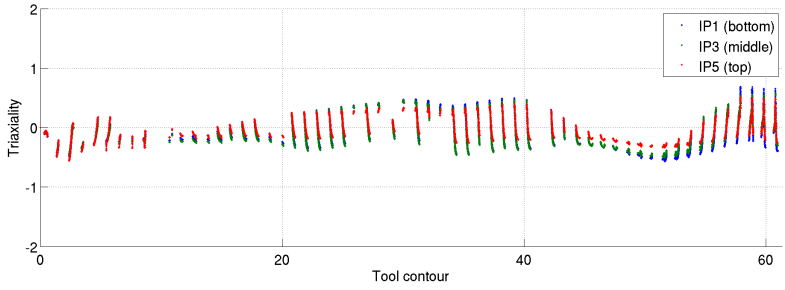

(b) Element 2.

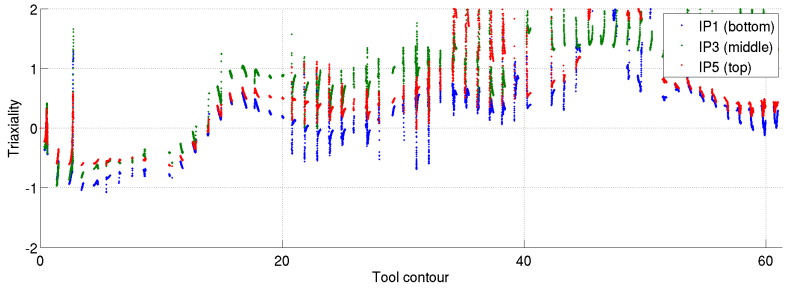

(c) Element 3.

Figure 11: Results for triaxiality.

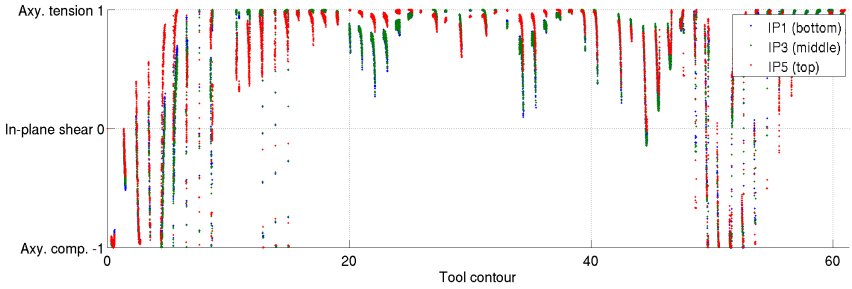

(a) Element 1.

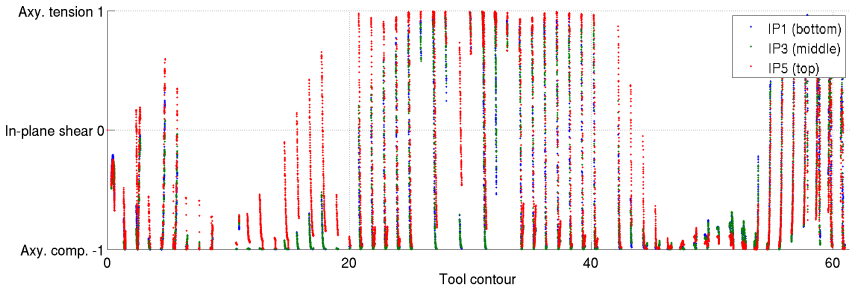

(b) Element 2.

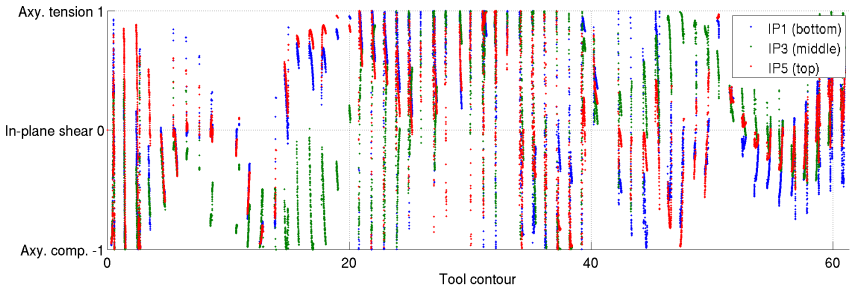

(c) Element 3.

Figure 12: Results for normalized third invariant.

3.2 Fine mesh, Set2

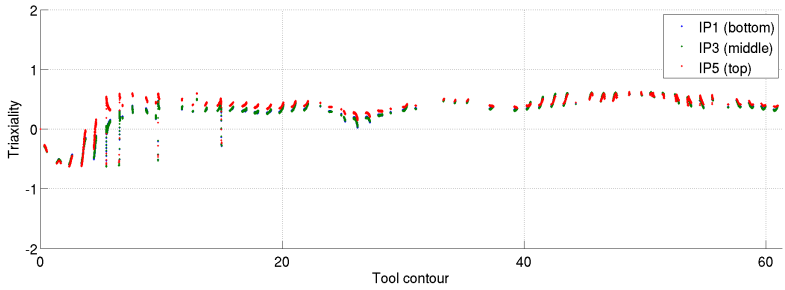

(a) Element 1.

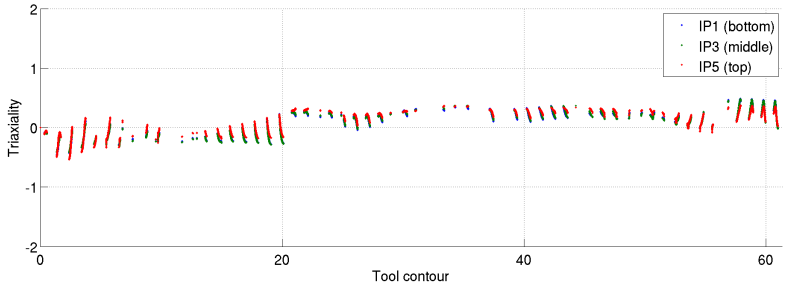

(b) Element 2.

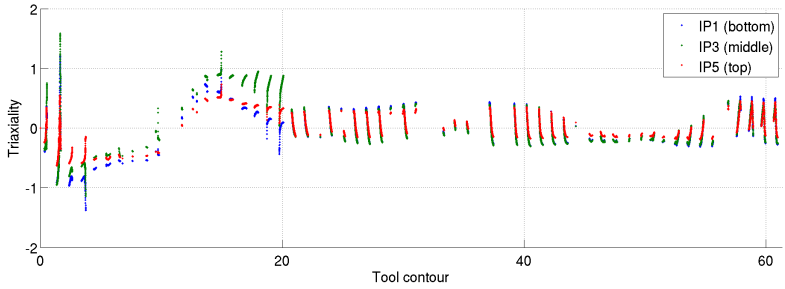

(c) Element 3.

Figure 13: Results for the triaxiality.

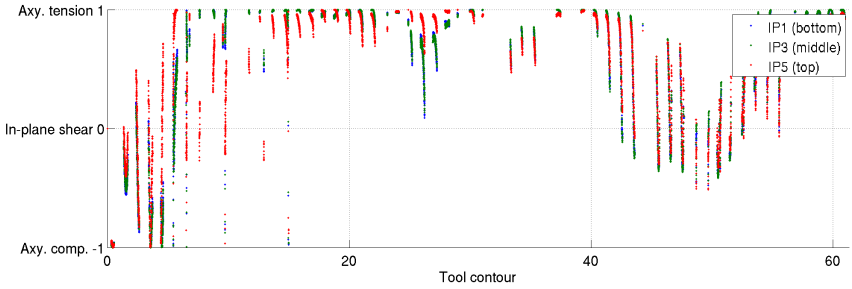

(a) Element 1.

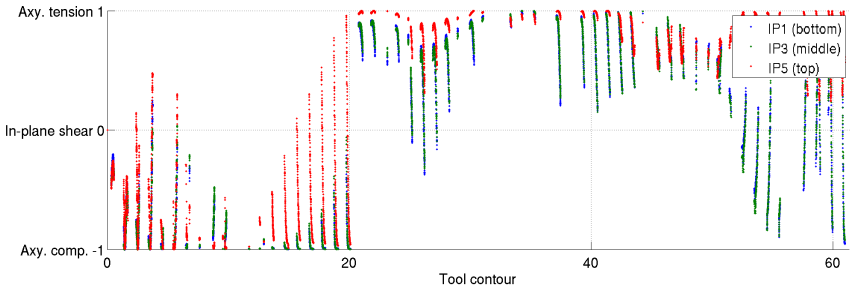

(b) Element 2.

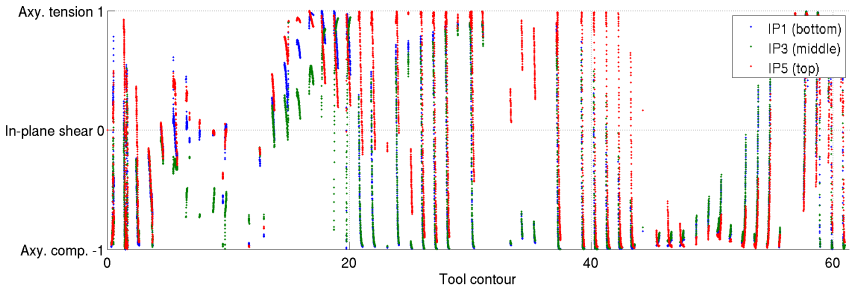

(c) Element 3.

Figure 14: Results for the normalized third invariant.

3.3 Analysis

For the elements far from the tool contact, the triaxiality remains near zero meaning that is a deviatoric state. During the tool contact, the triaxiality varies much more compare with elasticity, which remains steady. For a deeper analysis, in Fig. 15 the results for the fine mesh, are compared with the equivalent plastic strain. It is observed a sudden increase of the

triaxiality (*triaxiality peak*) when the tool is leaving the contact zone. This peak is also observed in the coarse mesh (Fig. 11(c)).

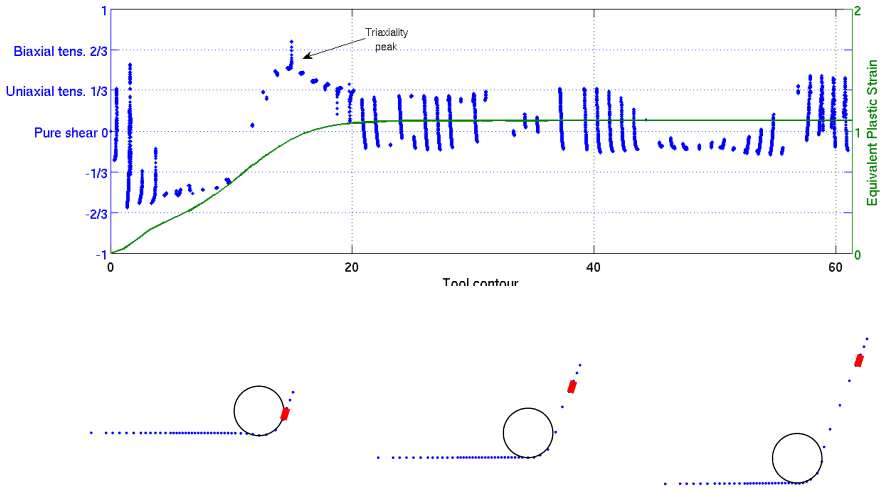

Figure 15: Triaxiality and equivalent plastic strain evolution for element 3, and the position of the element during the deformation.

The normalized third invariant exhibits high variance for all elements during one contour, making it difficult to get conclusions. This variance also implies a variable stress state, which depends in both in the tool position and the geometry (because the element in the flange is subjected to different stress state compared to the element under the tool). If the the Lode angle is obtained from triaxiality like in Eq. 3 (i.e., plane stress), and plotted in Fig. 16, it is remarkable how similar are both curves concluding that in elasticity the stress state is closer to plane stress, while in plasticity (or under the tool contact) is triaxial.

As element number 3 is deformed plastically too early during the process while element 2 start too late (Fig. 10), a new element (element 4) between these two is selected an analyzed during ten contours. The results for the triaxialiy are depicted in Fig. 17, showing that even if the level of deformation is the same that for element 3, the triaxiality is could be much higher during one contour.

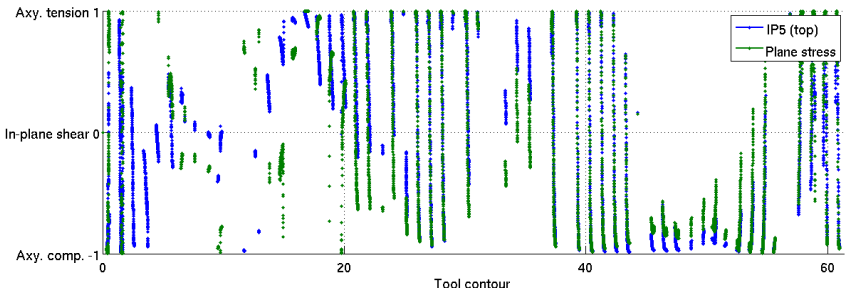

Figure 16: Lode angle plane for element 3.

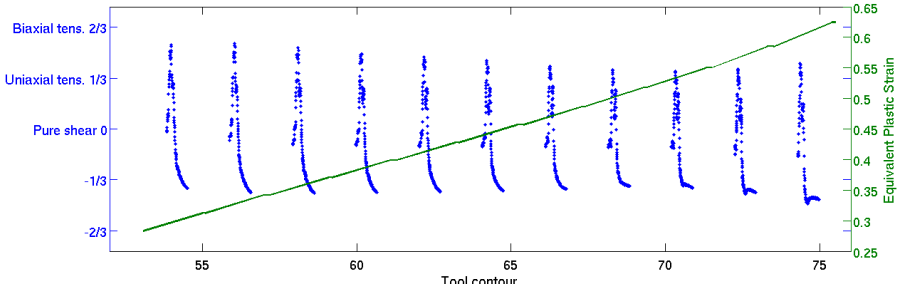

Figure 17: Triaxiality and equivalent plastic strain evolution on element 1756 during 10 contours.

References

J. Duflou, J. Verbert, B. Belkassem, J. Gu, H. Sol, C. Henrard, and A. M. Habraken. Process window enhancement for single point incremental forming through multi-step toolpaths. *CIRP Annals - Manufacturing Technology*, 57(1):253–256, 2008. ISSN 00078506. doi: 10.1016/j.cirp.2008.03.030. URL `http://linkinghub.elsevier.com/retrieve/pii/S0007850608000310`.

C. Henrard, C. Bouffioux, P. Eyckens, H. Sol, J. Duflou, P. van Houtte, A. Van Bael, L. Duchêne, and A. M. Habraken. Forming forces in single point incremental forming: prediction by finite element simulations, validation and sensitivity. *Computational Mechanics*, 47(5):573–590, Dec. 2010. ISSN 0178-7675. doi: 10.1007/s00466-010-0563-4. URL `http://www.springerlink.com/index/10.1007/s00466-010-0563-4`.